Flow boiling of R452A: heat transfer data, dry-out characteristics and a correlation

R. Mastrullo, A.W. Mauro*, L. Viscito

*Department of Industrial Engineering, Università degli studi di Napoli - Federico II, P.le Tecchio 80, 80125, Naples (Italy) - *email: alfonsowilliam.mauro@unina.it*

N.B.: This is the PREPRINT (submitted) version of this article. The final, published version of the article can be found at: https://doi.org/10.1016/j.expthermflusci.2019.04.006

Abstract

This paper presents an experimental investigation on two-phase heat transfer and dry-out occurrence for refrigerant R452A in a single horizontal circular stainless-steel tube having an internal diameter of 6.0 mm. The effects of mass flux (from 150 to 600 kg/m^{2}s), saturation (bubble) temperature (from 23 to 55 °C) and heat flux (from 10 to 65 kW/m^2) are investigated and discussed. Heat transfer coefficient and dry-out vapor quality data are then compared to R404A results in the same operating conditions, observing that the nucleate boiling contribution of the new blend is penalized by its very high glide temperature during evaporation. The assessment of some dry-out and flow boiling heat transfer coefficient prediction methods is finally carried-out and a correction factor on the nucleate boiling term is proposed to take into account the negative effect of the glide temperature difference on the mass diffusion in the liquid. By implementing this modification on two chosen asymptotic models, the statistical error analysis is considerably improved.

Keywords: R452A; R404A; flow boiling; glide effect; correlation.

Nomenclature

Roman

B	scaling factor	[-]
$\dot{Q}$	heat power	[W]
$\dot{m}$	mass flow rate	[kg/s]
c	specific heat	[J/kg K]
D	outer diameter	[m]
d	inner diameter	[m]
G	mass flux	[kg/m^2 s]
h	heat transfer coefficient	[W/m^2 K]
i	specific enthalpy	[J/kg]
I	current	[A]
L	length	[m]
L_h	total heated length	[m]
M	molecular mass	[kg/kmol]
n	number of samples	[-]
P	pressure	[Pa]
q	heat flux	[W/m^2]
S	suppression factor	[-]
T	temperature	[K]
V	voltage	[V]
x	vapor quality	[-]

Greek

Δ	variation	
α	exponent for heat transfer asymptotic models	[-]
β_L	liquid mass transfer coefficient	[m/s]
$\delta_{\pm 30\%}$	percentage of data points falling into a ±30% error band	%
λ	thermal conductivity	[W/m K]
μ	viscosity	[Pa s]
ρ	density	[kg/m^3]
σ	surface tension	[N/m]

Subscripts

B	bubble (saturation liquid)
bot	related to the bottom side
CB	convective boiling
exp	experimental
gl	glide
in	inlet
L	liquid
left	related to the left side
LV	liquid-to-vapor
mean	mean
mixt	mixture
NB	nucleate boiling
pred	predicted
preh	preheater
red	reduced
right	related to the right side
sat	saturation
th	related to the thermocouple measurement
top	related to the top side
tube	related to the tube
V	vapor
wall	related to wall

Dimensionless numbers and statistical parameters

$Bo = \frac{q}{G\Delta i_{LV}}$	Boiling number
$Pr = \frac{\mu c}{\lambda}$	Prandtl number
$ER = \frac{h_{pred} - h_{exp}}{h_{exp}} \cdot 100$	Error in prediction
$SD = \sqrt{\frac{1}{n}\sum_i (ER_i - MRE)^2}$	Standard Deviation
$MAE = \frac{1}{n}\sum_i \lvert ER_i \rvert$	Mean Absolute Error
$MRE = \frac{1}{n}\sum_i ER_i$	Mean Relative Error

Introduction

In the last decades, we are facing an unequivocal rise of the Earth surface and air temperature. According to the Fifth Assessment Report (AR5) of the Intergovernmental Panel on Climate Change (IPCC), the temperature has increased of 0.85 °C over the period 1880-2012 [1], and by lingering on this trend, the average rise may alarmingly reach 4 °C by 2100 [2] [3] [4] with severe drawbacks and extreme climate changes [5] [6].

Despite the ongoing debate in the scientific community about its causes and consequences [7], several studies [8] [9] have demonstrated that the contribution of vapor compression refrigeration systems using synthetic refrigerants on the global warming is significant. In fact, the Kigali Amendment to the Montreal Protocol established that, in order to avoid 0.5 °C in the global mean temperature by the XXI century, the HydroFluoroCarbon (HFC) production and consumption should be considerably reduced. This is mainly due to the direct greenhouse effect of the synthetic HFC refrigerants having a high Global Warming Potential (GWP), once they are released in atmosphere in case of leakages and/or improper plants dismantlement.

Among the fields of application, commercial refrigeration is one of the most critical sector [10] [11], due to the high amount of refrigerant charge required and the very high GWP value for R404A (equal to 3922), which is one of the most employed fluids [12]. According to the recent European restrictions and regulations for HFCs management [13], the chemical companies are now making significant efforts to find valuable alternatives, that have to be chosen by looking at their environmental impact, safety features and good adaptation to the required operating conditions.

As reviewed by Mota-Babiloni et al. [14], there is currently not a definitive solution to replace R404A, but several alternatives are under investigation, including HFC mixtures (R407A, R407F and R422A, having similar efficiency [15] but higher purchase costs [16]) and HFC/HFO (HydroFluoroOlephin) blends (as R448A, R449A and R452A). Particularly, R452A is a 3-component mixture made up of R32/R125/R1234yf at a composition of 11%/59%/30% by weight, designed to best match R404A's thermodynamic characteristics in order to become a retrofit substance in trucks and trailer refrigeration units [17], without a complete re-design of the compressor and other principal cycle components [18]. According to the ASHRAE [19] standards, R452A has been classified as A1 (non-toxic and non-flammable), with a zero-ODP (Ozone Depletion Potential) and a GWP value of 2141, thus complying with the 2500 GWP threshold value by 2020 given by the F-Gas Regulation for refrigerators and freezers for commercial use.

The retrofit operations of R452A in vapor compression cycles has been studied by Li [17], who performed a comprehensive investigation for the total lifetime CO_2-equivalent emissions for food transport refrigeration systems under various influencing factors. The author found that the use of R452A can make at least a 5-15% global emission reduction when compared to the baseline plant with R404A. Wang et al. [20] evaluated the optimal volume ratio of two-stage vapor compression systems by considering R452A among other 25 refrigerants. The optimal values of R452A were found to be slightly lower than those of R404A, as well as the system COP (3.82 versus 4.04, with evaporating/condensing temperatures of -5/+45 °C).

Besides these very limited overall system performance studies, experimental data on two-phase heat transfer characteristics for the new R452A blend would be of great use for the correct design of condensers and evaporators and also to provide an assessment of the existing prediction methods, that may not be effective when applied far from the operating conditions in which they were originally conceived. On this regard, only some R452A preliminary heat transfer and pressure drop data in limited working conditions were provided in our previous publication [21], and we did not find other works in scientific literature dealing with flow boiling of R452A and comparison with R404A.

The main objective of this paper is therefore to present a thorough experimental campaign on boiling heat transfer of refrigerants R452A and R404A, by collecting heat transfer coefficient and dry-out vapor quality data in a single horizontal stainless steel tube with an internal diameter of 6.0 mm. Tests have been performed by changing the refrigerants saturation (bubble) temperature from 23 to 55 °C, the mass flux from 150 to 600 kg/m^{2}s and the imposed heat flux from 10 to 65 kW/m^2, exploring all the vapor quality range, from the onset of boiling up to x =1. The experimental results have been firstly compared to R404A data at the same operating conditions, by exploring the differences related to both convective and nucleative boiling contributions. Finally, all data are compared with predicted

values of some correlations taken from literature, suggesting a modification that takes into account the negative glide temperature effect on the nucleation phenomenon.

Test rig

The sketch of the experimental facility used for the flow boiling experimental campaign is shown in Figure 1 (a photograph is provided in Figure 2), and has already been used for other published works by the same authors [22] [23]. The refrigerant loop is portrayed with a black line and runs clockwise, starting from the magnetic gear circulation pump (up to 2.5 dm^3/min) that pushes the subcooled liquid fluid into a Coriolis flow meter for the measurement of the mass flow rate. The subsequent pre-heating section is made up of a single copper tube and it is used to partially evaporate the liquid refrigerant up to a specific vapor quality before the measurement section, represented by a single stainless steel tube. The saturated fluid is finally condensed in a plate heat exchanger and sub-cooled in a tube-in-tube heat exchanger, before closing the loop with the pump suction head. Different transducers and sensors are placed throughout the main loop to record temperature and pressure. The mass flow rate into the tube test section is remotely controlled by changing the frequency of an inverter coupled with the pump electrical motor. Further adjustments during experiments are possible thanks to the main loop by-pass valve and also to the manually controlled throttling valves placed on the liquid and vapor lines. The saturation temperature is instead controlled by setting a specific temperature of the demineralized water flowing into the secondary loop (blue line in Figure 1) and feeding both the heat exchangers, via a remotely controlled thermostatic bath. More details on the test facility and of the whole equipment can be obtained from our previous publications [24] [25].

Test section and measurement equipment

The main characteristics of the test tube are resumed in Figure 2, whereas the measurement instrumentation with all the operative ranges and the related uncertainties are summarized in Table 1. The insulation material is made up of several layers of synthetic foam, preventing heat transfer to/from the environment. A single horizontal circular stainless steel (AISI316) tube is used for the present experimental campaign. The inner and outer diameters are repeatedly measured with an electronic caliper, giving values of 6.0±0.05 mm and 8.0±0.05 mm, respectively. According to the manufacturer, instead, the roughness of the inner surface is below 10 μm. The heat flux is imposed with an electrical DC voltage directly applied to the test tube thanks to two copper bars welded at a distance of 193.7±0.79 mm. The electrical resistance of the stainless steel heated section is estimated to be 5.1±0.084 Ω. Two measurement wires are then clamped at a distance of 101.6±0.41 mm for the evaluation of the applied heat flux, sufficiently far from the copper bars in order to guarantee the hypothesis of uniform heat flux. The DC voltage is measured with an analogical input module in the range 0-5 V, having an instrumental uncertainty of ±0.03% of the reading. The electrical current flowing into the test tube is instead directly measured with the DC power supply, having an overall uncertainty of ±1.0%. In the measurement point for the heat transfer coefficient, four T-type thermocouples are placed in this position at the top, bottom, left and right sides of the outer surface of the tube in order to have a better estimation of the average wall temperature. Their fastening is guaranteed with a high conductivity epoxy resin and a Kapton thin adhesive layer is used to electrically insulate the tube section from the sensors. All the thermocouples have been calibrated with a high precision resistance thermometer (RTD) and a thermostatic bath, giving an estimated maximum uncertainty of ±0.1 °C. Two pressure taps are right outside the heated length, in order to measure the inlet absolute pressure (within 0/35 bar range, carrying an overall uncertainty of ±0.1% of the reading) and the total pressure drop across the test section (with a calibrated differential pressure transducer having a maximum instrumental uncertainty of ±0.06 kPa). The refrigerant mass flow rate in the test section is obtained by a Coriolis mass flow meter (from 2.3 to 115.7 g/s) with an overall uncertainty of ±1.0% of the reading. Finally, the heat power given to the pre-heating section to have a specific vapor quality in the test tube is instead measured with an analogic wattmeter (from 0 to 3.6 kW) having an instrumental uncertainty of ±1.0%.

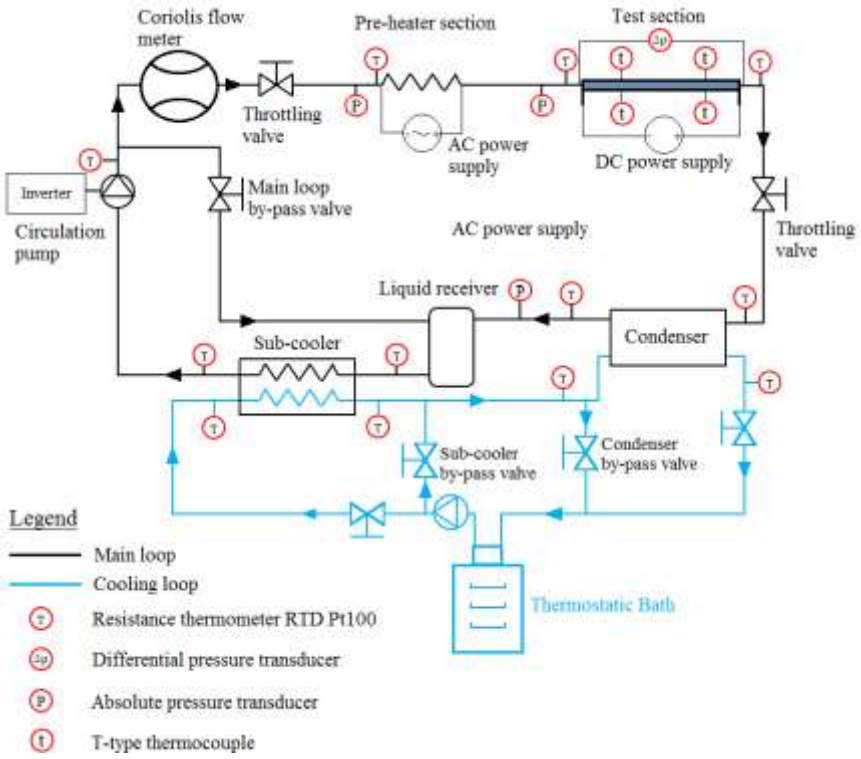

Figure 1 Sketch of the test facility used for the flow boiling experiments

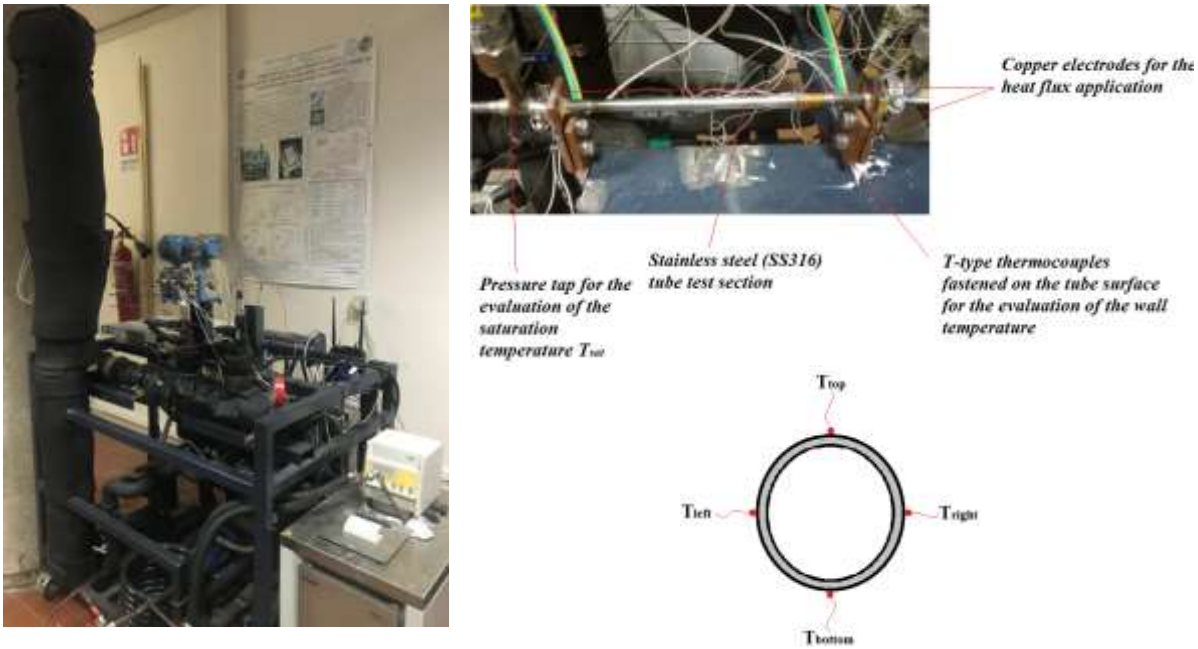

Figure 2 Photograph of the test rig and test section main features

Table 1 Summary of the measurement instrumentation

Measurement	Range	Instrument accuracy

Temperature (4-wire Pt100 RTD)	-80/250 °C	±0.180 °C
Wall temperature (T-type thermocouples)	5/85 °C	±0.10 °C
Inlet absolute pressure	0/35 bar	±0.1 % reading
Absolute pressure	0/50 bar	±0.3 % reading
Differential pressure	0/14.51 kPa	±0.06 kPa
Flow meter	2.3/115.7 g/s	±1 % reading
Electrical power (pre-heater)	0/3.6 kW	±1 % reading
Voltage (test section)	0/5 V	±0.03 % reading
Current (test section)	0/300 A	±1 % reading

Method

Data reduction

The mean heat transfer coefficient is obtained by considering a uniform heat flux q and an average wall temperature from the four measurement points:

$$h_{mean} = \frac{q}{T_{wall} - T_{sat}} = \frac{V \cdot I}{\pi d L_h} \cdot \frac{1}{T_{wall} - T_{sat}} \tag{1}$$

$$T_{wall} = \frac{T_{wall,top} + T_{wall,bottom} + T_{wall,left} + T_{wall,right}}{4} \tag{2}$$

The inner wall temperature T_{wall} is obtained from the measured outer wall temperature T_{th} with the hypothesis of 1-D heat transfer in the radial direction, uniform heat generation and homogeneous and isotropic material of the test tube. The thermal conductivity of the stainless-steel λ_{tube} is assumed to be 16.23 W/mK, having a very limited variation in the range of temperatures investigated. The inner and outer diameter are referred as d and D, respectively.

$$T_{wall} = T_{th} + \frac{V \cdot I}{4\pi\lambda_{tube} L_h} \cdot \frac{\left(\frac{D}{d}\right)^2 \cdot \left(1 - \ln\left(\left(\frac{D}{d}\right)^2\right)\right) - 1}{\left(\frac{D}{d}\right)^2 - 1} \tag{3}$$

As the local vapor quality, the actual fluid temperature T_{sat} at the measurement point is a function of both pressure P and enthalpy i, being refrigerant R452A a non-azeotropic blend with significant glide temperature for all the operating conditions investigated.

$$T_{sat} = f(P,i) \tag{4}$$

The fluid pressure is estimated by measuring the inlet pressure and the total pressure drop, by considering a constant pressure gradient in the heated section. The enthalpy i, instead, is obtained from an energy balance applied to the test tube from the inlet of the diabatic section up to the measurement point. In turn, the inlet enthalpy i_{in} is calculated with an energy balance applied to the pre-heating section. The pre-heater inlet enthalpy $i_{in,preh}$ is finally directly obtained as a function of the measured temperature and absolute pressure of the sub-cooled liquid refrigerant.

$$i = i_{in} + \frac{4 \cdot L \cdot q}{G \cdot d} \tag{5}$$

$$i_{in} = i_{in,preh} + \frac{\dot{Q}_{preh}}{\dot{m}} \tag{6}$$

All the thermodynamic and transport properties of refrigerants R452A and R404A are collected with the software Refprop 9.1, developed by NIST [26], while the data reduction process has been performed with MATLAB software [27].

Uncertainty analysis, test procedure and preliminary tests

The uncertainty of all the measured parameters has been evaluated by composing the instrumental uncertainty to the unavoidable bias during experiments. The resulting combined uncertainties of the measured parameters are then composed by means of the law of propagation of error by Moffat [28] to achieve the combined uncertainty for the derived parameters (operating conditions and results). A coverage factor $z = 2$ is eventually used to build an expanded uncertainty that assures a confidence level higher than 95%. A summary of the uncertainty analysis for various parameters is provided in Table 2, in which the entire database is split in two parts. There are from one side (almost 90% of the data points) the typical boiling conditions, in which the system is stable and the bias is very limited. When approaching the dry-out and with post-dry-out heat transfer (roughly 10% of the database), there are inevitable wider mass flow rate and wall temperature fluctuations due to the chaotic physics of the phenomenon itself. For this reason, the overall uncertainty in this case can be considerably higher.

Each test is performed and saved in steady state conditions, by fixing the mass flux, heat flux and system pressure. It is worth noting that, for refrigerants such as R452A having a considerable glide during evaporation, a constant system pressure is not equivalent to a constant saturation temperature. From 10 to 15 data points are then taken from the lowest vapor quality approaching the saturated liquid condition up to the dry-out occurrence and post-dry-out heat transfer. The test is finally stopped either when the saturated vapor conditions are reached (x =1) or when the wall temperatures reach the highest threshold of 85 °C, in order not to compromise the chemical stability of the insulating foam. To ensure the steady state conditions during experiments and to build a high-quality database, the uncertainty of operating parameters was calculated in real-time and the data acquisition could start only when the standard deviation of the working conditions during the recording time of 90 seconds was inferior to a chosen threshold. The uncertainty limits are ±0.2 °C for the wall temperatures, ±3% for the mass flux and ±0.10 °C for the (liquid) saturation temperature.

Some preliminary tests have been performed with sub-cooled refrigerant R134a in order to verify the correct insulation of the pre-heating and measurement section. Specifically, the energy balance on the pre-heater revealed that the heat losses could be calculated as a simple linear function of the temperature difference between the heated section and the surrounding environment. As regards the test section, besides the adiabaticity tests in which the heat losses were found to be negligible, the single-phase heat transfer coefficients were also evaluated and compared to the well known correlation of Dittus-Boelter [29] for turbulent flow, giving a fair agreement. More details on this preliminary tests and their results is available in some of our previous publications [22] [30] [31].

Table 2 Uncertainty of operating parameters and heat transfer coefficient

Parameter	**Maximum uncertainty for 90% of the database**	**Maximum recorded uncertainty (dry-out conditions)**
Saturation temperature T_{sat}	±0.08 °C	±0.12 °C
Mass flux G	±1.6%	±4.5%
Heat flux q	±0.71%	±0.78%
Vapor quality x	±0.02	±0.16
Mean heat transfer coefficient h_{mean}	±7.3%	±14%

Heat transfer coefficient results

Effect of operating parameters

The local heat transfer coefficients of refrigerant R452A are presented in this section as a function of the vapor quality, by investigating the effect of the operating parameters in terms of mass flux (varied from 150 to 600 kg/m^{2}s), imposed heat flux (from 10 to 65 kW/m^2) and saturation pressure (from 12 to 25 bar). The saturation temperatures displayed in all the following diagrams refer to the bubble (x=0) temperature at a specific pressure. The error bands for the experimental heat transfer coefficients are

related to the instrumental uncertainties and titles and legends are intended to be averaged among all the corresponding values.

The effect of the mass flux on the cross sectional average heat transfer coefficient at a bubble temperature of 23.6 °C and an imposed heat flux of 10 kW/m^2 is shown in Figure 3a. A typical convective behavior is found for medium and high mass fluxes, with an increasing heat transfer coefficient with ongoing evaporation and higher values for higher mass fluxes, especially for vapor qualities above 0.20. A different, decreasing trend is shown instead for the lowest mass flux of 150 kg/m^{2}s, suggesting a possible flow stratification for such a low inertia. This hypothesis is corroborated by looking at the local heat transfer coefficients evaluated at the top and bottom side of the test tube, respectively in Figure 3b-c. Starting from a vapor quality of approximately 0.20, the liquid phase is only able to wet the bottom part of the tube, whereas the vapor stays at the top, strongly reducing the corresponding heat transfer coefficient. This behavior was also observed for the same mass flux at different operating conditions. Another point worth noting for the mass fluxes of 400 and 600 kg/m^{2}s is that the top heat transfer coefficient is always higher (10-50%) than its corresponding bottom value, suggesting a non-symmetric annular flow. Finally, at G=600 kg/m^{2}s, the bottom heat transfer coefficient reaches its peak at a vapor quality of 0.90, in which the top heat transfer performance has already fallen caused by the dry-out occurrence.

a)

b)

c)

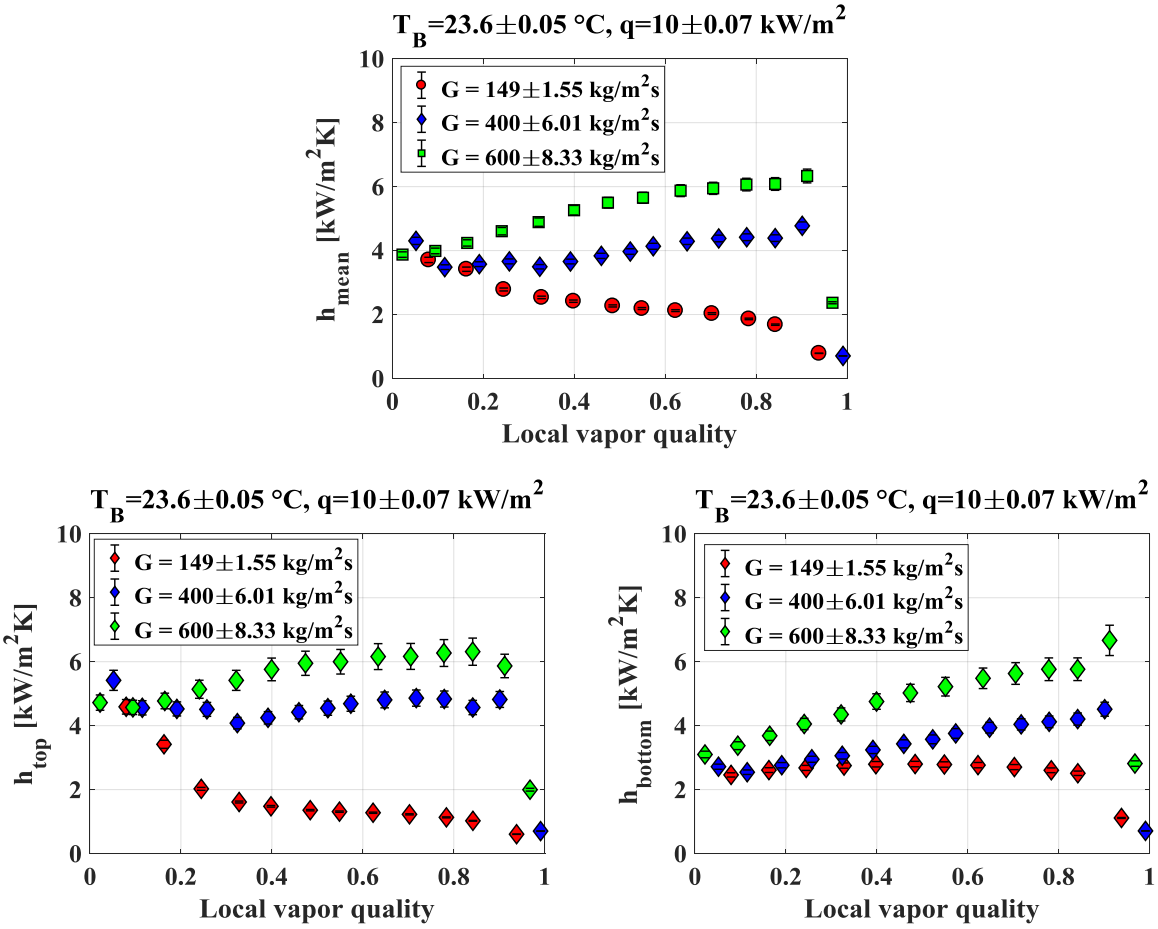

Figure 3 Effect of the mass flux on the R452A boiling heat transfer coefficient. (a) Cross sectional average heat transfer coefficient. (b) Top heat transfer coefficient. (c) Bottom heat transfer coefficient

The effect of the bubble temperature on the cross sectional average heat transfer coefficient at an imposed heat flux of 10 kW/m^2 and two different mass velocities is shown in Figure 4a-b. For the highest mass flux of 600 kg/m^{2}s (Figure 4a), the saturation temperature does not provide any significant effect on the average heat transfer coefficient increasing trend with vapor quality, up to 54 °C, at which there is a possible change of flow pattern. With an increasing reduced pressure, in fact,

besides having more similar liquid and vapor velocities due to the approach of the phase densities, the reduction of the surface tension also concurs to have a more unstable liquid film on the top wall, resulting in an anticipated dry-out and a decreasing trend with vapor quality. For the lowest mass flux of 150 kg/m^{2}s (Figure 4b), this behavior is found for all the bubble temperatures investigated, due to the low inertia which cannot hold up the liquid phase on the top wall. Also in this case, the average heat transfer coefficient is not significantly influenced by a change of the saturation pressure.

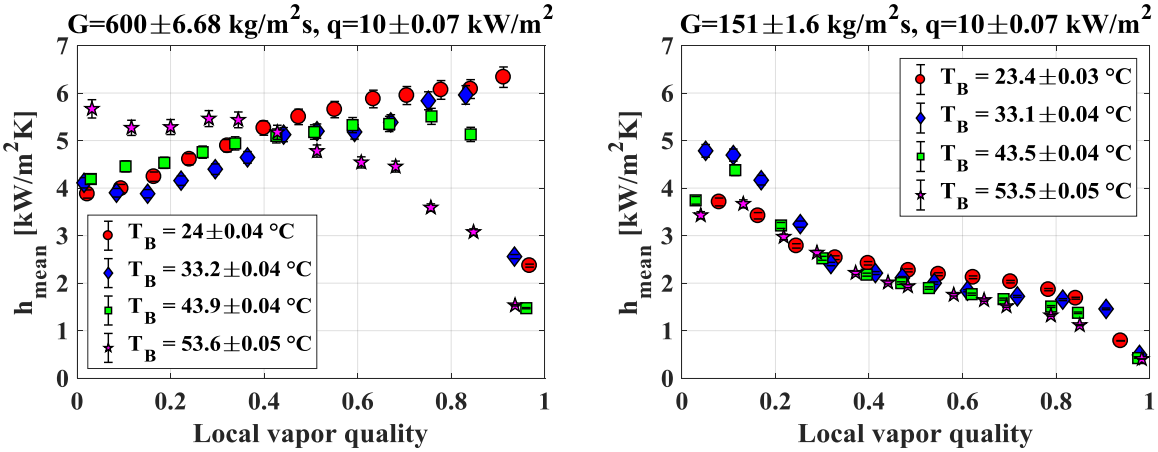

Figure 4 Effect of the bubble saturation temperature for a high (a) and low (b) mass flux, with an imposed heat flux of 10 kW/m^2.

The effect of the imposed heat flux at a bubble temperature of 33.2 °C and a mass flux of 598 kg/m^{2}s is shown in Figure 5a-c for the average heat transfer coefficient and local top and bottom data, respectively. With an increasing heat flux, there is a remarkable increase (>100%) of the average values and a reduction of their slope with vapor quality, suggesting the predominance of the nucleate boiling contribution at higher *q*, which is also observed for the bottom heat transfer coefficient values (Figure 5c). At 40 kW/m^2, there is a significant drop starting from a vapor quality of approximately 0.50, due to the dry-out occurrence at the top side of the tube, as shown in Figure 5b, whereas the bottom values remain quite high up to the definitive dry-out completion, occurring roughly at *x*=0.80.

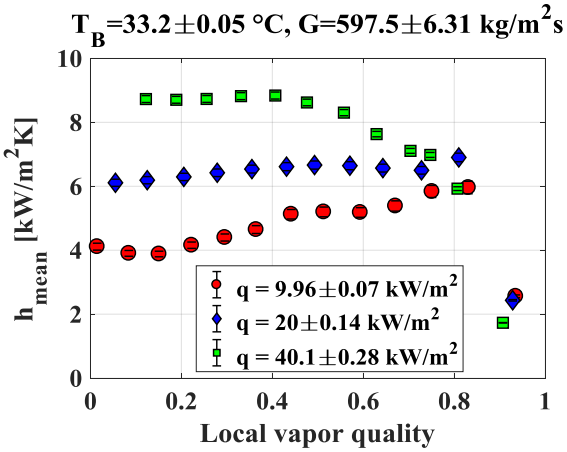

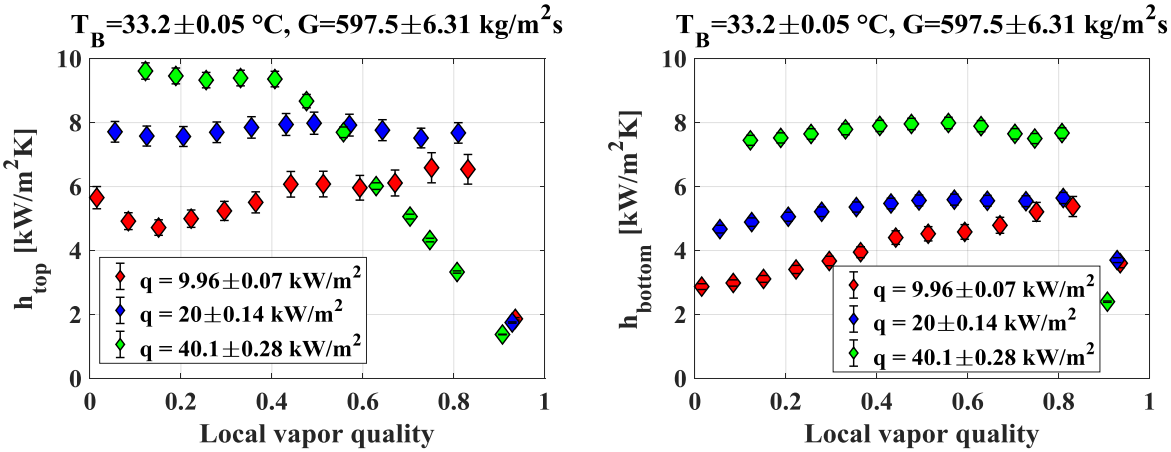

Figure 5 Effect of the heat flux on the R452A boiling heat transfer coefficient. (a) Cross sectional average heat transfer coefficient. (b) Top heat transfer coefficient. (c) Bottom heat transfer coefficient

b) c)

Comparison with R404A in convective and nucleative driven conditions

The cross sectional average heat transfer coefficients at a bubble temperature of 24 °C and an imposed heat flux of 10 kW/m^2 are shown in Figure 6 for both refrigerants. In case of convective-driven heat transfer (at 600 kg/m^{2}s), the heat transfer coefficients of both fluids share the same slope with vapor quality and also comparable values. This is explained by looking at the very similar thermodynamic and transport properties of the two refrigerants at a saturation pressure of 12 bar in Table 3, especially in terms of liquid thermal conductivity, saturated vapor density and vapor-to-liquid density ratio. The first is accountable for the conduction heat transfer through the liquid film, and the latter are responsible for the flow acceleration during evaporation and therefore for the convective contribution to the flow boiling heat transfer. In case of negligible convection and predominant nucleate boiling heat transfer (at 150 kg/m^{2}s), the heat transfer coefficients of R404A are instead always significantly higher than the corresponding values for R452A. This behavior can be in part justified with the slightly higher liquid Prandtl number and reduced pressure for refrigerant R404A. However, it is worth noting that R404A is a quasi-azeotropic mixture, having a very small glide of 0.4 °C at 12 bar, whereas the increase of the saturation temperature from saturated liquid to vapor is almost ten times higher for R452A, negatively affecting the nucleate boiling contribution. As described by Carey [32], when vaporization occurs in a non-azeotropic blend, the generated vapor is richer in the more volatile component than the bulk liquid, whereas the corresponding concentration of the remaining liquid close to the interface is lower. As a consequence, the more volatile component diffuses in the liquid towards the interface, whereas the excess less volatile component drifts away in the bulk liquid. This implies that the actual interface temperature is then higher than that of the initial bubble temperature. Therefore, the driving wall superheat for supplying heat to the interface is lower than that based on the bubble point, on which the heat transfer coefficient is conventionally defined, resulting in its reduction as a function of the glide temperature of the mixture.

Table 3 Main thermodynamic properties for refrigerants R452A and R404A at a pressure of 12 bar

Fluid	$T_{sat,L}$ [°C]	$T_{sat,V}$ [°C]	P_{red} [-]	ρ_V/ρ_L [-]	ρ_V [kg/m^3]	ρ_L [kg/m^3]	λ_L [W/mK]	Pr_L	σ [10^3 N/m]	μ_L [10^5 Pa s]
R452A	23.3	27.0	0.301	0.0566	64.5	1139	0.068	3.01	5.19	14.2
R404A	23.3	23.7	0.321	0.0598	62.9	1052	0.064	3.12	4.69	13.1

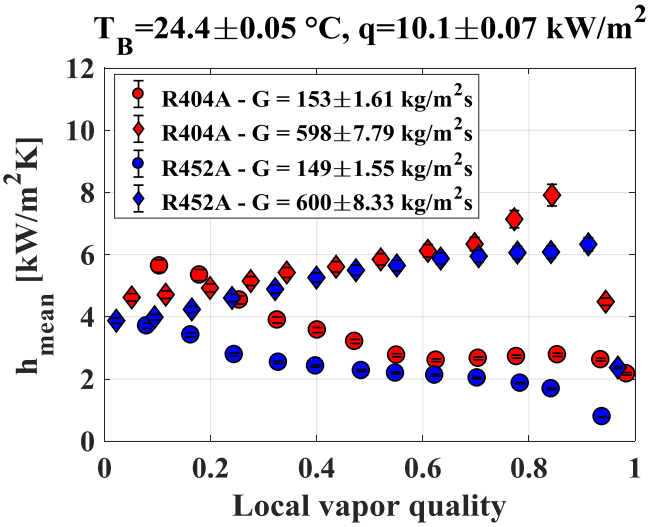

Figure 6 Boiling heat transfer coefficients of R452A and R404A for two mass fluxes of 150 and 600 kg/m^{2}s.

Effect of the mass transfer resistance to the nucleate boiling heat transfer

For a deeper insight of the glide effect on the nucleate boiling heat transfer, Figure 7 shows the bottom heat transfer coefficients for both R452A and R404A at a mass flux of 400 kg/m^{2}s and a bubble temperature of 34 °C. The choice of the bottom values better complies with the present analysis on the isolation of the nucleate boiling contribution, thanks to their almost constant trend with vapor quality, differently from the top heat transfer coefficients, that may either have a non-negligible convective contribution (at medium-high mass velocities) or a decreasing trend with vapor quality due to a change of the liquid film distribution (intermittent flow regime, asymmetric annular flow regime or dry-out).

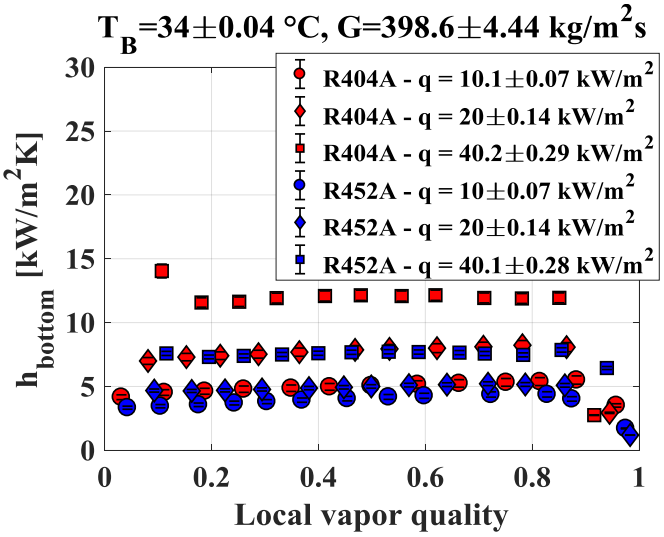

Figure 7 Bottom heat transfer coefficients of R452A (in blue) and R404A (in red) with increasing imposed heat flux.

According to the asymptotic approach used in numerous prediction methods, the heat transfer coefficient can be expressed as a function of both nucleate and convective boiling contributions, as in Eq. (7):

$$h = \left(h_{NB}^{\alpha} + h_{CB}^{\alpha}\right)^{1/\alpha} \tag{7}$$

In order to segregate the effect of the mass composition of the liquid on the nucleate boiling heat transfer coefficient h_{NB}, this last term has to be isolated. By using a reference state h_0, with the

hypothesis of a constant convective contribution h_{CB} with varying heat flux, it is possible to fairly approximate the ratio of the nucleate boiling contribution to the ratio of the overall heat transfer coefficient as shown in Eq. (8), as far as the convective contribution is not predominant in the heat transfer process. The mathematical construction of Eq. (8) with the abovementioned hypotheses is described in detail in Appendix.

$$\frac{h_{NB}}{h_{NB,0}} \cong \frac{h}{h_0} \tag{8}$$

In case of a pure fluid or a quasi-azeotropic mixture, the nucleate boiling heat transfer coefficient is typically a function of the heat flux to the power of a rational number included within 0.60 and 0.90 [33] [34] [35] [36] [37]. By considering the well-known and widely used correlation of Cooper [33], the nucleate boiling heat transfer coefficient ratio with respect to the reference state can be written as:

$$\frac{h_{NB}}{h_{NB,0}} = \left(\frac{q}{q_0}\right)^{0.67} \tag{9}$$

For a non-azeotropic mixture, such as R452A, different authors have proposed a modification of the typical nucleate boiling contribution by taking into account the resistance to mass diffusion in the liquid, as reviewed by Grauso et al. [38]. One of the most applied correction factors is that by Thome and Shakir [39], that reads as in Eq. (10). The parameter B is a scaling factor relating the fraction of total heat flux converted to latent heat, generally assumed equal to 1.0, β_L is the liquid mass transfer coefficient, generally set to 0.0003 m/s (found to be varying from 0.0001 to 0.0005 m/s), ΔT_{gl} is the glide temperature and h_{NB} is the ideal heat transfer coefficient, that by excluding the convective contribution, may still be evaluated with the typical Cooper expression for pure fluids.

$$\frac{h_{NB,mixt}}{h_{NB,0,mixt}} = \left(\frac{q}{q_0}\right)^{0.67} \cdot \left[\frac{\left(1+\frac{h_{NB}\Delta T_{gl}}{q}\left(1-e^{-\frac{B}{\beta_L}\frac{q}{\Delta i_{LV}\rho_L}}\right)\right)^{-1}}{\left(1+\frac{h_{NB,0}\Delta T_{gl}}{q_0}\left(1-e^{-\frac{B}{\beta_L}\frac{q_0}{\Delta i_{LV}\rho_L}}\right)\right)^{-1}}\right] \tag{10}$$

Figure 8 shows the effect of the heat flux variation for the bottom heat transfer coefficients of R404A (Figure 8a) and R452A (Figure 8b). As mentioned beforehand, the bottom heat transfer coefficients are a fair representation of the only nucleate boiling contribution, since they are not significantly dependent on the vapor quality variation. For each operating condition in terms of mass flux and bubble temperature, all the experimental values are divided by the reference value ($h_{bott,0}$) referred to the lowest heat flux of 10 kW/m^2. Besides the experimental data, the solid blue line corresponds to the Cooper-based heat flux influence on the heat transfer coefficient (Eq. (9)), whereas the dashed lines refer to the Cooper-based effect corrected by the Thome and Shakir [39] factor, as in Eq. (10). The non-unique line for the glide correction trend takes into account the effect of the saturation temperature on Eq. (10). Even with a non-perfect agreement, the experimental data for R404A are better crossed by using the Cooper correlation for pure fluids, and a lower effect of the heat flux variation is found for R452A points, that are fairly predicted with the Thome and Shakir correction for high-glide mixtures.

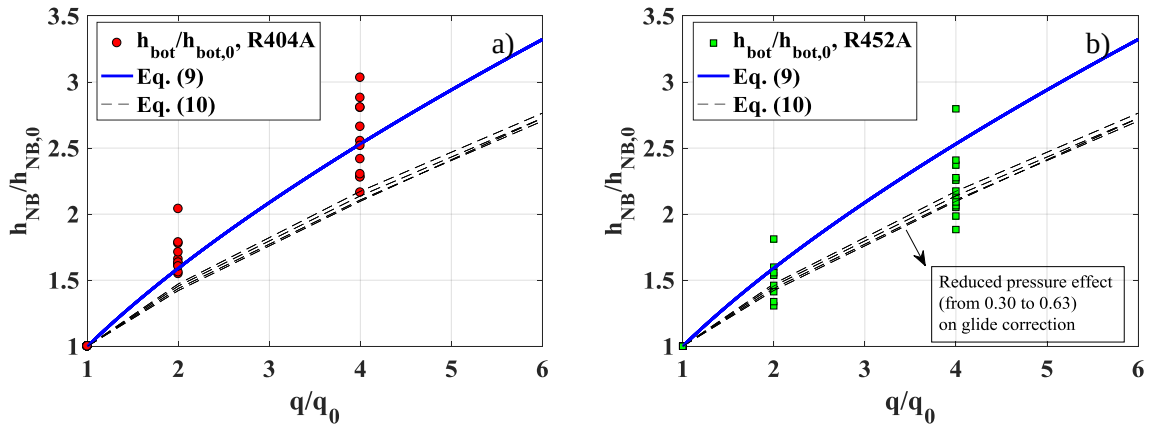

Figure 8 Effect of heat flux variation on the bottom heat transfer coefficients for R404A (a) and R452A (b) and comparison with Cooper **[33]** expression and Thome and Shakir **[39]** correction for non-azeotropic mixtures.

Assessment of predictive methods and nucleate boiling modification according to the glide effect

The R452A average heat transfer coefficient results have been compared to some correlations taken from literature. The statistical parameters Mean Absolute and Relative Errors (*MAE*, *MRE*), Standard Deviation (*SD*) and the percentage of data points falling into an error band of ±30% ($\delta_{\pm 30\%}$), all defined in nomenclature, are used for the statistical analysis. The complete assessment with the evaluation of the statistical parameters is given in Table 4, whereas the experimental trends with vapor quality at two different operating conditions are displayed and compared with some chosen correlations in Figure 9a-b.

In case of convective-driven heat transfer, at G=600 kg/m^{2}s and a low heat flux and saturation temperature (Figure 9a), the asymptotic (α=2) prediction method of Liu and Winterton [40] and the algebraic turbulence model (developed for annular flow) of Cioncolini and Thome [41] underestimate the experimental data. The correlation of Del Col [42], built as a modification of the Gungor and Winterton [43] method, overestimates instead the results for most vapor qualities. The remaining superimposition model of Gungor and Winterton [43], and the asymptotic correlations of Kim and Mudawar [44] (α=2) and Wjotan et al. [45] (α=3) provide instead a good agreement, slightly overpredicting the experimental data. The latter, being a flow pattern based method, is also able to catch the dry-out occurrence and to define the sudden drop of the heat transfer coefficient at high vapor quality.

In case of low convection, at G=150 kg/m^{2}s and a higher saturation temperature (Figure 9b), most of the predictive methods significantly overestimate the experimental values, and only the correlations of Gungor and Winterton [43], Kim and Mudawar [44] and Wjotan et al. [45] are able to chase the descending heat transfer coefficient trend with vapor quality.

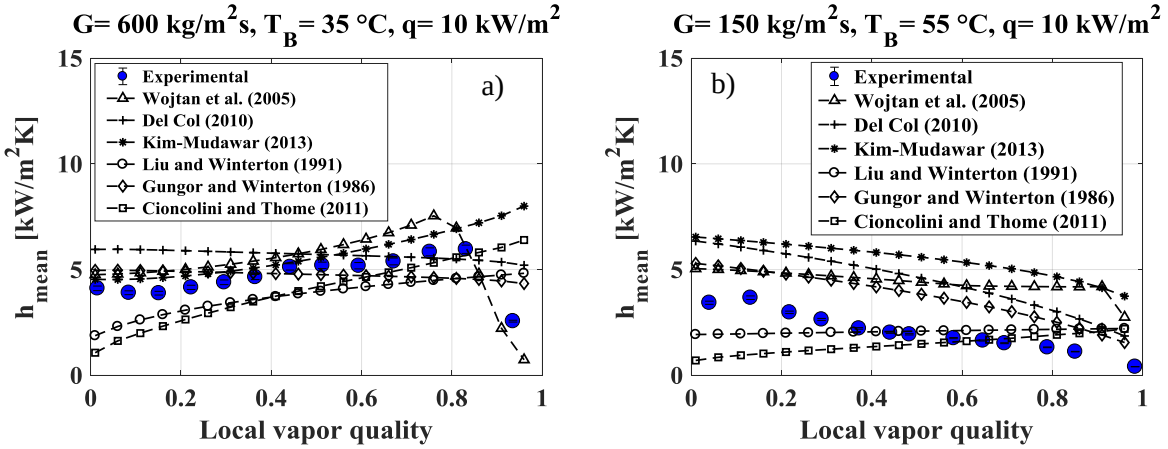

Figure 9 Predicted and experimental average heat transfer coefficient trends with vapor quality. (a) G=600 kg/m^{2}s, T_B=35 °C and q=10 kW/m^2, (b) G=150 kg/m^{2}s, T_B=55 °C and q=10 kW/m^2.

Table 4 Assessment of all the chosen two-phase heat transfer coefficient prediction methods. Bold numbers refer to the best values

Author	MAE	MRE	SD	$\delta_{\pm 30\%}$
Bertsch et al. [46]	52.9	45.2	45.6	40.4
Lazarek-Black [47]	59.7	31.8	48.8	41.7
Chen [48]	53.5	5.0	56.7	40.5
Liu-Winterton [40]	52.2	-26.3	34.6	37.2
Cioncolini-Thome [41]	55.3	-38.6	33.8	29.2
Gungor-Winterton [43]	**49.2**	28.9	40.3	**52.6**
Kandlikar-Balasubramanian [49]	75.2	64.8	59.7	23.5
Del Col [42]	52.0	59.0	43.4	47.7
Kim-Mudawar [44]	**47.1**	38.3	45.1	**53.8**
Wojtan et al. [45]	**51.1**	31.1	48.8	**53.5**

The two asymptotic models of Kim and Mudawar [44] and of Wojtan et al. [45] that better managed to replicate the experimental trends for all the operating conditions have been modified according to the previous analysis on the negative effect of the glide temperature on the nucleate boiling contribution. Specifically, the general expression of the heat transfer coefficient for both methods is that of Eq. (7), in which the exponent α is equal to 2 and 3, respectively. Due to their length and complexity, the complete mathematical formulation of both methods is not reported here and can be found in the original references.

The original nucleate boiling contribution for the Kim and Mudawar correlation [44] is a function of the Boiling number Bo, the reduced pressure P_{red}, the vapor quality x and the liquid heat transfer coefficient h_L from the Dittus-Boelter equation [29], as shown in Eq. (11):

$$h_{NB,Kim-Mud} = 2345 Bo^{0.7} P_{red}^{0.38} (1-x)^{-0.51} h_L \tag{11}$$

The flow pattern based method of Wojtan et al. [45], instead, considers the typical Cooper correlation for pool boiling multiplied by a constant suppression factor S equal to 0.8, as shown in Eq. (12):

$$h_{NB,Wojtan} = S \cdot \left(55 P_{red}^{0.12} (-\log(P_{red}))^{-0.55} M^{-0.5} q^{0.67}\right) \quad (12)$$

The nucleative boiling expressions of Eqs. (11) and (12) have been eventually corrected with the Thome and Shakir [39] factor, in which the ideal heat transfer coefficient h_{id} is calculated with the Cooper formula [33], as shown in Eq. (13)

$$h_{NB,mod} = h_{NB} \cdot \left(1 + \frac{h_{id} \Delta T_{gl}}{q}\left(1 - e^{-\frac{B}{\beta_L}\frac{q}{\Delta i_{LV} \rho_L}}\right)\right)^{-1} \quad (13)$$

The effect of the modification based on the glide effect is graphically shown in Figure 10a-d. For both correlations, the assessment has improved with a significant reduction of the mean errors and a considerable increase of the percentage of data points falling into an error range of ±30%, that becomes 62.4% and 63.0%, respectively.

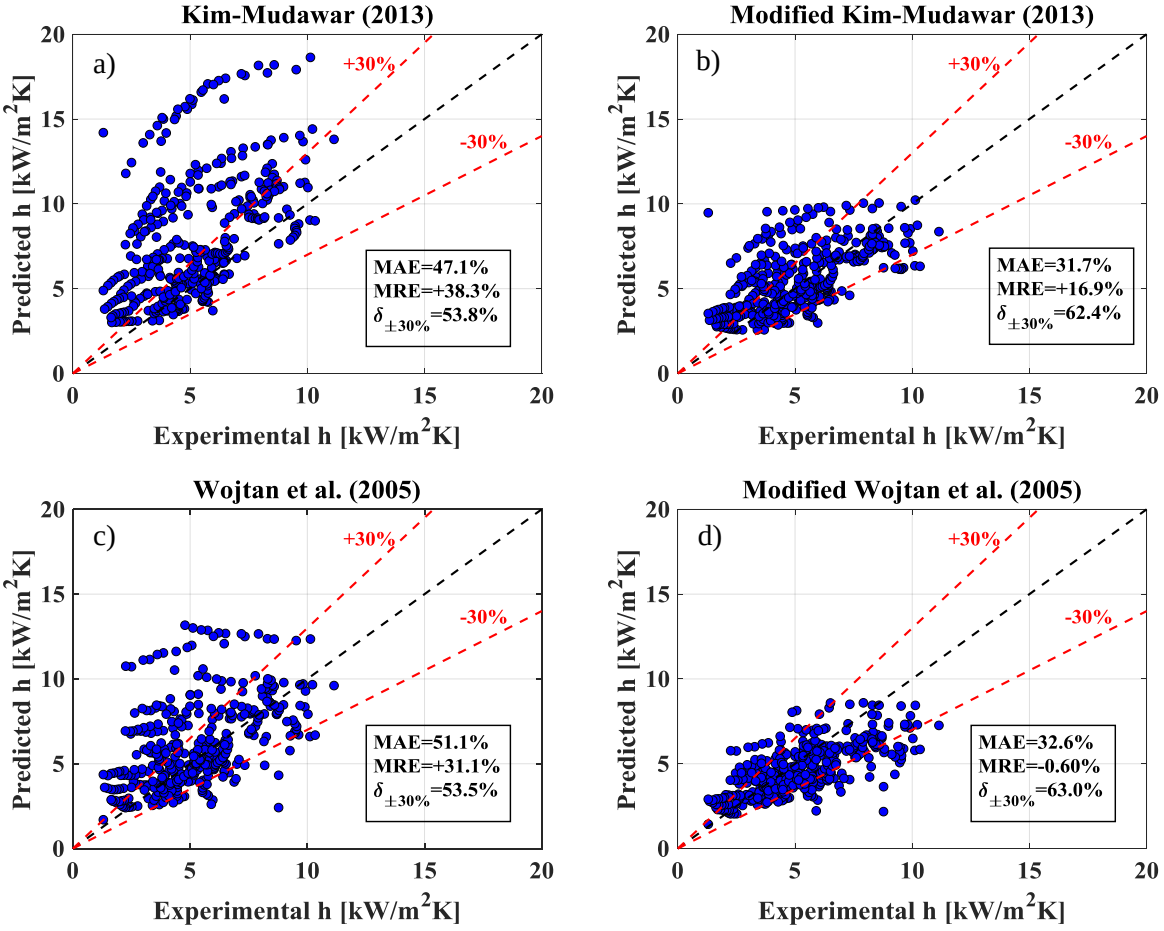

Figure 10 Experimental versus predicted average R452A two-phase heat transfer coefficients. (a) Original Kim and Mudawar **[44]**. (b) Modified Kim and Mudawar. (c) Original Wojtan et al. **[45]**.(d) Modified Wojtan et al.

Dry-out vapor quality results and assessment

Experimental results

In all fields of application, the correct design of evaporators requires the knowledge of the vapor quality at the onset of dry-out. In this condition, typically occurring at high vapor qualities, the heat transfer performance suddenly drops due to the lack of the liquid phase at the heated wall. While for vertical tubes and uniform applied heat fluxes the dry-out phenomenon appears simultaneously on the whole wall perimeter, in case of a horizontal channel disposition the dry-out firstly occurs at the top side of the wall due to stratification effects and gradually reaches other parts of the tube perimeter. For

this work, the vapor quality at the dry-out occurrence is determined as the last point before the calculated heat transfer coefficient at the top drops more than 10% from its previous value. An analogous approach has also been used in the paper of Wojtan et al. [50] and Diani et al. [51].
The same operating conditions of the R452A heat transfer coefficient results were used to extrapolate 25 dry-out vapor quality data from the boiling curves. Tests at G=150 kg/m^{2}s were not considered, since the flow is likely to be stratified and the top heat transfer coefficient always drops down immediately at very low vapor qualities, as shown in Figure 3. The combined effect of the heat flux, mass flux and saturation temperature on the dry-out incipience vapor quality is shown in Figure 11a-b. The general trends show a decreasing dry-out vapor quality with increasing heat flux. At G = 600 kg/m^2 s and 35 °C, the dry-out vapor quality passes from 0.83 to 0.62 when the heat flux is set from 10 to 40 kW/m^2, and other examples are available for all the operating conditions. From the data at disposal, the change of mass flux returns a negligible influence on the occurrence of dry-out, and no speculations are possible (see Figure 11a). From Figure 11b, instead, there is a general reduction of the dry-out vapor quality with increasing bubble temperature, possibly due to a reduction of the fluid surface tension that tries to hold up the liquid film. The R452A dry-out vapor quality trends with heat flux are then compared with the R404A points obtained at a mass flux of 400 kg/m^{2}s and a bubble temperature of 55 °C in Figure 11c. The two fluids share substantially similar dry-out results, even if R404A shows a slightly anticipated dry-out with respect to R452A, possibly due to a higher reduced pressure and a lower surface tension for the same operating conditions, as already presented in Table 3.

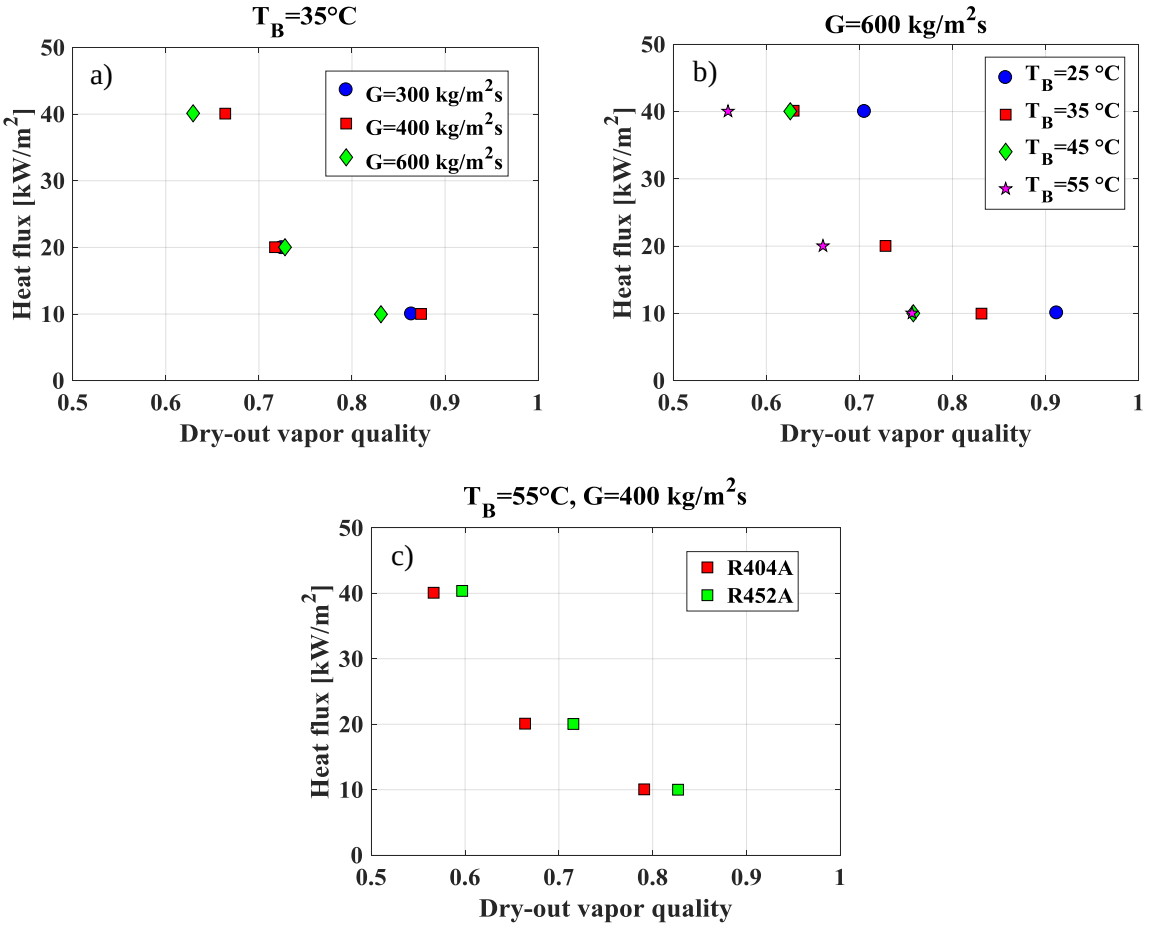

Figure 11 Imposed heat flux as a function of the dry-out vapor quality. (a) Effect of the mass flux for a saturation temperature of 25 °C. (b) Effect of the saturation temperature for a mass flux of 220 kg/m^{2}s. (c) Comparison with R404A data at a mass flux of 400 kg/m^{2}s and a bubble temperature of 55 °C

Assessment of correlations
The experimental dry-out data are compared with six correlations taken from literature, concerning different fluids, diameters and ranges of operating conditions. Particularly, Kim and Mudawar [52]

prediction method has been developed for halogenated refrigerants, water and carbon dioxide for small diameters up to 6.0 mm internal diameter and a wide range of mass fluxes and reduced pressures. The correlations of Ducoulombier et al. [53] and of Cheng et al. [54] were instead conceived for CO_2, the first for minichannels (d = 0.529 mm) and the latter for mini and conventional tubes (0.8-10.0 mm). In the flow pattern map of Wojtan et al. [50], the authors modified the original Mori et al. [55] expression by including the heat flux effect for the evaluation of the dry-out incipience vapor quality. Their database included experiments with R22 and R410A with macrochannels of 8.00 mm and 13.84 mm. Del Col et al. [56] also developed a dry-out incipience vapor quality correlation for minichannels working with refrigerants and CO_2 and finally Mastrullo et al. [57] conceived a new flow pattern map based on the effect of the reduced pressure on the flow regimes transition zones. From their method, the evaluation of the dry-out vapor quality is extrapolated for the present assessment. Further details on the mathematical expression of these correlations and their applicability range are available in the reference mentioned.

The experimental and predicted dry-out vapor quality trends with imposed heat flux is presented in Figure 12a-b. For a low bubble temperature of 25 °C, all the correlations provide similar values and decreasing trends at higher heat fluxes, with the best agreement found with Kim and Mudawar [52] and Wojtan et al. [50]. The latter keeps on working very well also for a higher saturation temperature of 55 °C (Figure 12b), while most of the remaining correlations underestimate the dry-out vapor quality. The largest discrepancies are always found with the methods of Cheng et al. [54] and Ducoulombier et al. [53], that are however conceived only for carbon dioxide at very high reduced pressure, thus far from the operating conditions explored in this paper.

Table 5 presents a summary of the assessment for dry-out vapor quality prediction methods with the evaluation of all the statistical parameters, whereas a graphical comparison between predicted and experimental dry-out data for the best working correlations of Kim and Mudawar [52] and Wojtan et al. [50] is provided in Figure 12a-b, respectively. In the first case, the calculated *MAE* is 16.4%, with $\delta_{\pm 30\%}$=68%, whereas the second correlation has a very low *MAE* of 6.6%, with almost all the data points falling into an error range of ±30%.

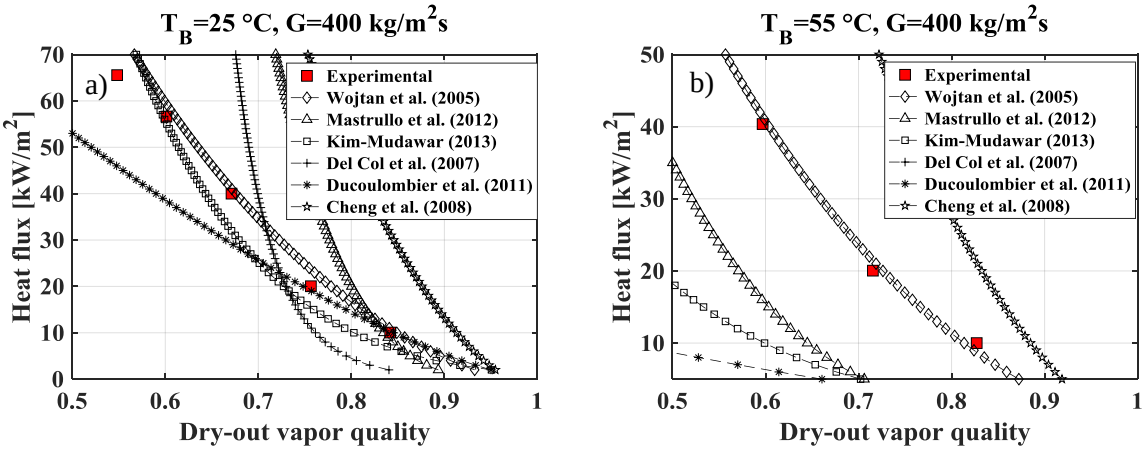

Figure 12 Predicted and experimental dry-out vapor qualities with imposed heat flux. (a) G=400 kg/m^{2}s, T_B=25 °C. (b) G=400 kg/m^{2}s, T_B=55 °C.

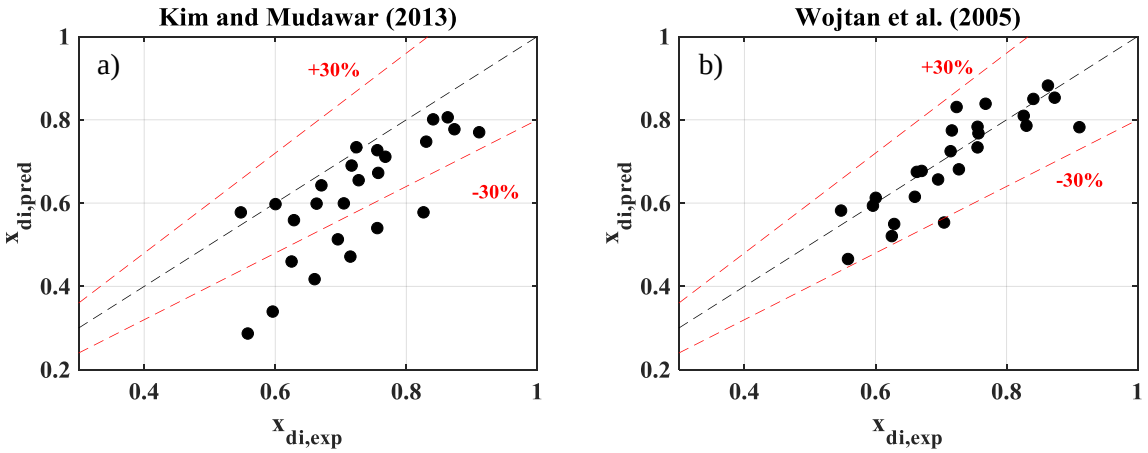

Figure 13 Experimental versus predicted R452A dry-out vapor quality data. (a) Correlation of Kim and Mudawar **[52]**. (b) Flow pattern based method of Wojtan et al. **[50]**.

Table 5 Summary of comparisons with the chosen dry-out incipience vapor quality correlations. Bold numbers refer to the best values

Author	MAE	MRE	SD	$\delta_{\pm 30\%}$
Wojtan et al. [50]	**6.6**	-2.7	8.5	**96.0**
Del Col et al. [56]	28.0	-24.9	22.5	44.0
Cheng et al. [54]	16.6	16.4	8.7	64.0
Ducoulombier et al. [53]	36.6	-36.6	43.6	56.0
Mastrullo et al. [57]	20.3	-11.5	24.3	56.0
Kim and Mudawar [52]	**16.4**	-15.9	14.1	**68.0**

Conclusions

An experimental analysis on the two-phase boiling heat transfer of refrigerant R452A has been carried-out in a single horizontal circular tube with an internal diameter of 6.0 mm. The effect of the operating parameters and a critical comparison with R404A data are performed, by quantifying the effect of the glide temperature difference on the nucleate boiling heat transfer. Finally, the agreement of the dry-out vapor quality and heat transfer coefficient existing correlation is also assessed.
The main outcomes of this research are summarized as follows:

- A convective behavior of the R452A heat transfer coefficient is found for the highest investigated mass fluxes, starting from 400 kg/m^{2}s. Similar trends and values are also observed for refrigerant R404A due to their alike thermodynamic and transport properties.
- The saturation temperature does not significantly affect the average R452A heat transfer coefficients, except for the cases in which it is likely to establish a change of flow pattern, as observed for the highest bubble temperature of 55 °C at a mass flux of 600 kg/m^{2}s.
- The heat flux has a positive effect on the R452A heat transfer coefficient. However, its influence is clearly reduced with respect to R404A results at the same operating conditions, that instead show a typical Cooper-based ($\propto q^{0.67}$) influence. The main reason has been attributed to the large glide temperature of R452A, leading to a mass diffusion resistance in the liquid, thus negatively affecting the nucleate boiling contribution to the heat transfer. This effect is successfully quantified for the present experimental database with the Thome and Shakir [39] correction.
- The assessment of two-phase heat transfer predictive methods has shown that the asymptotic correlations of Kim and Mudawar [44] and of Wojtan et al. [45] might be considerably

improved by applying the correction factor developed by Thome and Shakir [39] on the nucleate boiling term, thus taking into account the glide temperature effect.

- The dry-out occurrence for R452A and R404A was found to be anticipated with increasing heat flux, whereas mass flux and saturation temperature do not show a significant effect. Among the chosen prediction methods for dry-out vapor quality, the correlation of Kim and Mudawar [52] and the flow pattern map of Wojtan et al. [50] better fit the experimental data, providing a *MAE* of 16.4% and 6.6%, respectively.

Acknowledgements

Luca Viscito received a grant at Federico II University funded by "Ministero dell'Istruzione dell'Università e della Ricerca", via the project PRIN2015 "Clean Heating and Cooling Technologies For An Energy Efficient Smart Grid", which is gratefully acknowledged.

Appendix

A consistent amount of two-phase heat transfer prediction methods exploit an asymptotic approach, in which the overall heat transfer coefficient may be written as a function of the convective and nucleate boiling contributions, using a positive exponent α>1, typically equal to 2 or 3:

$$h = \left(h_{NB}^{\alpha} + h_{CB}^{\alpha}\right)^{1/\alpha} \tag{14}$$

With the definition of a reference state h_0, Eq. (14) can read as:

$$\frac{h_{NB}}{h_{NB,0}} = \frac{h}{h_0}\left(\frac{1-h_{CB}^{\alpha}h^{-\alpha}}{1-h_{CB,0}^{\alpha}h_0^{-\alpha}}\right)^{1/\alpha} \tag{15}$$

By considering the sole variation of the heat flux between the actual condition and the reference state, it is fair to assume that the convective boiling contribution remains constant ($h_{CB} = h_{CB,0}$). The ratio of the nucleate boiling terms can be therefore rewritten in Eq. (16) as a function of the overall heat transfer coefficients ratio and a correction parameter *C*, which is dependent on the relative importance of the convective boiling term.

$$\frac{h_{NB}}{h_{NB,0}} = \frac{h}{h_0}\left(\frac{1-h_{CB,0}^{\alpha}h^{-\alpha}}{1-h_{CB,0}^{\alpha}h_0^{-\alpha}}\right)^{1/\alpha} = \frac{h}{h_0}\cdot C \tag{16}$$

Figure 14 shows the nucleate boiling heat transfer coefficient ratio for three different enhancement of the overall heat transfer performance (1.2, 2 and 4) with increasing heat flux. All curves are plotted as a function of the relative importance of the convective boiling contribution, for an exponent α=2.
In all the three cases, for convective heat transfer shares lower than 50%, the correction parameter *C* is very close to 1.0 and can be neglected. This is a fair assumption especially when considering heat transfer coefficients at the bottom side of the tube at low mass velocities, as in the example in Figure 7, for which Eq. (17) might be considered:

$$\frac{h_{NB}}{h_{NB,0}} \cong \frac{h}{h_0} \quad \text{for } \frac{h_{CB,0}}{h_0} < 0.5 \tag{17}$$

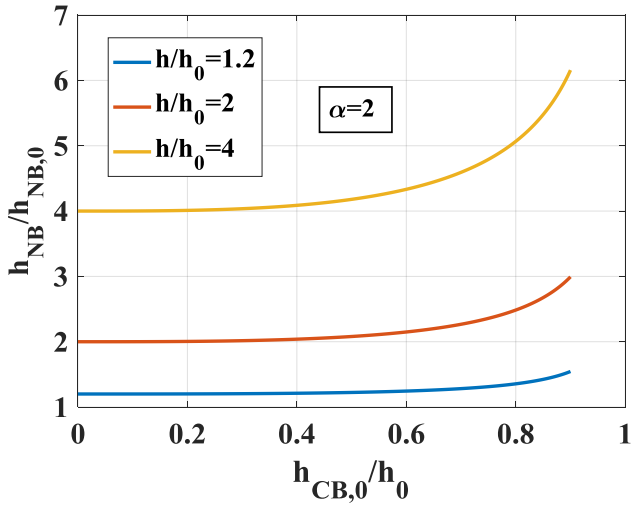

Figure 14 Nucleate boiling heat transfer coefficients ratio as a function of the relative importance of the convective boiling contribution, as shown in Eq. (16)

References

[1] T.F. Stocker, Contribution of working group I to the fift assessment report of the intergovernmental panel on climate change, Cambridge University Press, Cambridge (2013).

[2] R.A. Betts, M. Collins, D.L. Hemming, C.D. Jones, J.A. Lowe, M.G. Sanderson, When could global warming reach 4 °C?, Phil. Trans. R. Soc. (2011) 67-84 https://doi.org/10.1098/rsta.2010.0292.

[3] M.G. Sanderson, D.L. Hemming, R.A. Betts, Regional temperature and precipitation changes under high-end (>4 °C) global warming, Phil. Trans. R. Soc. A 369 (2011), 85-98, https://doi.org/10.1098/rsta.2010.0283.

[4] R. James, R. Washington, Changes in African temperature and precipitation associated with degrees of global warming, Clim Change 117 (2013) 859-872.

[5] X. Wang, D. Jiang, X. Lang, Future extreme cliamte changes linked to global warming intensity, Science Bulletin 62 (2017) 1673-1680.

[6] I.I. Berchin, I.B. Valduga, J. Garcia, J.B.S. Osorio de Andrade Guerra, Climate change and forced migrations: an effort towards recognizing climate refugees, Geoforum 84 (2017) 147-150.

[7] C.A. Varotsos, M.N. Efstathiou, Has global warming already arrived?, J. Athmospheric Solar-Terrestrial Physics 182 (2019) 31-38.

[8] N. Abas, A.R. Kalair, N. Khan, A. Haider, Z. Saleem, M.S. Saleem, Natural and synthetic refrigerants, global warming: A review, Renewable Sustainable Energy Reviews 90 (2018) 557-569.

[9] S. Choi, J. Oh, Y. Hwang, H. Lee, Life cycle climate performance evaluation (LCCP) on cooling and heating systems in South Korea, Appl. Therm. En. 120 (2017) 88-98.

[10] J.A. Evans, E.C. Hammond, A.J. Gigiel, A.M. Fostera, L. Reinholdt, K. Fikiin, C. Zilio, Assessment of methods to reduce the energy consumption of food cold stores, Appl. Th. Eng. 62 (2014) 697-705.

[11] C. Francis, G. Maidment, G. Davies, An investigation of refrigerant leakage in commercial refrigeration, Int. J. Refrigeration 74 (2017) 12-21.

[12] B.J. Cardoso, F. B. Lamas, A.R. Gaspar, J.B. Ribeiro, Refrigerants used in the Portuguese food industry: current status, Int. J. Refrigeration 83 (2017) 60-74.

[13] Regulation (EU) No 517/2014 of the European Parliament and the Council of 16 April 2014 fluorinated greenhouse gases and repealing Regulation (CE) No 842/2006. Off. J. Union.

[14] A. Mota-Babiloni, J. Navarro-Esbri, A. Barragan-Cervera, F. Molés, B. Peris, G. Verdu, Commercial refrigeration - An overview of current status, Int. J. Refrigeration 57 (2015) 186-196.

[15] M. Bortolini, M. Gamberi, R. Gamberini, A. Graziani, F. Lolli, A. Regattieri, Retrofitting of R404A commercial refrigeration systems using R410A and R407F refrigerants, Int. J. Refr. 55 (2015) 142-152.

[16] A. Maratou, EU policy update - F-Gas Regulation, HFC taxes & fiscal incentives for natural refrigerants. In: ATMOshpere Asia 2014 - Technology and Innovation, Tokyo, Japan, 3-5 February 2015.

[17] G. Li, Comprehensive investigation of transport refrigeration life cycle climate performance, Sust. En. Techn. and Assessments 21 (2017) 33-49.

[18] Z. Marek, J- Sedliak, F-Gases EU Regulation: R404A Replacement Refrigerants - Compressor Manufacturer Experience (2015).

[19] American Society of Heating, Refrigerating and Air-Conditioning Engineers, Inc. ASHRAE Standard 34 Designation and Safety Classification of Refrigerants; 2013.

[20] B. Wang, Z. Cheng, W. Shi, X. Li, Optimal volume ratio of two-stage vapour compression system using zeotropic refrigerant, Int. J. Refrigeration (2018) https://doi.org/10.1016/j.ijrefrig.2018.11.021.

[21] G. Lillo, R. Mastrullo, A.W. Mauro, L. Viscito, Flow boiling data of R452A, Energy Procedia 148 (2018) 1034-1041.

[22] G. Lillo, R. Mastrullo, A.W. Mauro, L. Viscito, Flow boiling heat transfer, dry-out vapor quality and pressure drop of propane (R290): Experiments and assessment of predictive methods, Int. J. Heat Mass Transfer 126 (2018) 1236-1252.

[23] G. Lillo, R. Mastrullo, A.W. Mauro, L. Viscito, Flow boiling of R1233zd(E) in a horizontal tube: Experiments, assessment and correlation for asymmetric annular flow, Int. J. Heat Mass Transfer 129 (2019) 547-561.

[24] G. Lillo, R. Mastrullo, A.W. Mauro, L. Viscito, Flow boiling of R32 in a horizontal stainless steel tube with 6.00 mm ID. Experiments, assessment of correlations and comparison with refrigerant R410A, Int. J. Refrigeration 97 (2019) 143-156.

[25] R. Mastrullo, A.W. Mauro, R. Revellin, L. Viscito, Flow boiling heat transfer and pressure drop of pure ethanol (99.8%) in a horizontal stainless steel tube at low reduced pressures, Appl Therm Eng 145 (2918) 251-263.

[26] Lemmon E W, Mc M.O. Linden, M.L. Huber, REFPROP NIST Standard Reference Database 23, Version 9.0, 2009.

[27] MATLAB release. Natick, Massachussets, United States, The MathWorks, Inc..

[28] R.J. Moffat, Using uncertainty analysis in the planning of an experiment. Transactions of the ASME: Journal of Fluids Engineering 107 (1985) 173–178..

[29] F.W. Dittus, L.M.K. Boelter, Heat transfer in automobile radiators of the tubular type, Univ. Calif. Publ. Eng. 2 (1930) 443-461.

[30] R. Mastrullo, A.W. Mauro, L. Viscito, Flow boiling of R32 in a horizontal smooth tube of 6.0 mm internal diameter: heat transfer coefficient and pressure drop, Journal of Physics: Conf. Series 923 (2017) 012015.

[31] G. Lillo, R. Mastrullo, A.W. Mauro, L. Viscito, Experimental study of flow boiling of propane in a 6mm internal diameter horizontal tube, Refrig Science and Technology, June-2018, 798-806 http://dx.doi.org/10.18462/iir.gl.2018.1278.

[32] V.P. Carey, Liquid-vapor phase-change phenomena - An introduction to the thermophysics of vaporization and condensation processes in heat transfer equipment, Washington D.C.: Hemisphere Publishing Corporation, 1992.

[33] M. Cooper, Heat flow rates in saturated nucleate pool boiling - wide-ranging examination using reduced properties, Advances in Heat Transfer 16 (1984) 157-239.

[34] K. Stephan, M.A. Abdelsalam, Heat transfer correlations for natural convection boiling, Int. J. Heat Mass Transfer 23 (1980), 73-87.

[35] D. Gorenflo, Pool Boiling, VDI-HEat Atlas, VDI-Verlag, Dusseldorf (English Version), 1993.

[36] I.L. Mostinski, Application of the rule of corresponding states for calculation of heat transfer and critical heat flux to boiling liquids, British Chemical Engineering Abstracts, FOLIO no. 150 (1963), 580.

[37] G. Ribatski, J.M. Saiz Jabardo, Experimental study of nucleate boiling of halocarbon refrigerants on cylindrical surfaces, Int. J. Heat Mass Transfer 46 (2003) 4439-4451.

[38] S. Grauso, R. Mastrullo, A.W. Mauro, G.P. Vanoli, CO2 and propane blends: Experiments and assessment of predictive methods for flow boiling in horizontal tubes, Int. J. Refrigeration 34 (2011) 1028-1039.

[39] J.R. Thome, S. Shakir, A new correlation for nucleate pool boiling of aqueous mixtures, AIChE Symp. Ser. 83 (1987) 46-51.

[40] Z. Liu, R.H.S. Winterton, A General correlation for saturated and subcooled flow boiling in tubes and annuli, based on a nucleate pool boiling equation, Int. J. Heat Mass Trans. 34 (1991) 2759-2766.

[41] A. Cioncolini, J.R. Thome, Algebraic turbulence modeling in adiabatic and evaporating annular two-phase flow, Int. J. Heat Fluid Flow 32 (2011) 805–817.

[42] D. Del Col, Flow boiling of halogenated refrigerants at high saturation temperature in a horizontal smooth tube. Exp. Th. Fluid Science 34 (2010) 234-245.

[43] K. Gungor, R. Winterton, A general correlation for flow boiling in tubes and annuli, Int. J. Heat Mass trans. 29 (1986) 351-358.

[44] S.M. Kim, I. Mudawar, Universal approach to predicting saturated flow boiling heat transfer in mini/micro-channels - Part II. Two-phase heat transfer coefficient, Int. J. Heat Mass Trans. 64 (2013) 1239-1256.

[45] L. Wojtan, T. Ursenbacher, J.R. Thome, Investigation of flow boiling in horizontal tubes: Part II - developement of a new heat transfer model for stratified-wavy, dryout and mist flow regimes, Int. J. Heat Mass Transfer 48 (2005) 2970-2985.

[46] S.S. Bertsch, E.A. Groll, S.V. Garimella, A composite heat transfer correlation for saturated flow boiling in small channels, Int. J. Heat Mass Transfer 52 (2009) 2110-2118.

[47] G.M. Lazarek, S.H. Black, Evaporative heat transfer, pressure drop and critical heat flux in a small vertical tube with R-113, Int J Heat Mass Trans 25 (1982) 945-960.

[48] J.C. Chen, Correlation for boiling heat transfer to saturated fluids in convective flow, Ind. Eng. Chem. Process Design and Development 5 (1966) 332-329.

[49] S.G. Kandlikar, P. Balasubramanian, An experimental study in the effect of gravitational orientation on flow boiling of water in 1054x197 μm parallel minichannels, J. Heat Transfer 127 (2005) 820-829.

[50] L. Wojtan, T. Ursenbacher, J.R. Thome, Investigation of flow boiling in horizontal tubes: Part I - A new diabatic two-phase flow pattern map, Int. J. Heat Mass Trans. 48 (2005) 2955-2969.

[51] A. Diani, S. Mancin, L. Rossetto, R1234ze(E) flow boiling inside a 3.4 mm ID microfin tube, Int. J. Refr. 47 (2014) 105-119.

[52] S.M. Kim, I. Mudawar, Universal approach to predicting saturated flow boiling heat transfer in mini/micro-channels - Part I. Dry-out incipience quality, Int. J. Heat Mass Trans. 64 (2013) 1226-1238.

[53] M. Ducoulombier, S. Colasson, J. Bonjour, P. Haberschill, Carbon dioxide flow boiling in a single microchannel - Part II: Heat transfer, Exp. Th. Fluid Sc. 35 (2011) 591-611.

[54] L. Cheng, G. Ribatski, J.M. quiben, J.R. Thome, New prediction methods for CO2 evaporation inside tubes: Part I - A two-phase flow pattern map and a flow pattern based phenomenological model for two-phase flow frictional pressure drops,, Int. J. Heat Mass Trans. 51 (2008) 111-124.

[55] H. Mori, S. Yoshida, K. Ohishi, Y. Kokimoto, Dryout quality and post dryout heat transfer coefficient in horizontal evaporator tubes, in: Proc. of the 3rd European Thermal Sciences Conference (2000), pp. 839-844.

[56] D. Del Col, F. Fantini, L. Rossetto, Dryout quality in a minichannel flow boiling, XXV UIT National Heat Transfer Conference, Italy (2007), pp. 18-20.

[57] R. Mastrullo, A.W. Mauro, J.R. Thome, D. Toto, G.P. Vanoli, Flow pattern maps for convective boiling of CO2 and R410A in a horizontal smooth tube: experiments and new correlations analyzing the effect of the reduced pressure, Int. J. Heat Mass Trans. 55, (2012) 1519-1528.